PHYSICAL REVIEW A **86**, 051404(R) (2012)

Determination of the $5d6s\ ^3D_1$ state lifetime and blackbody-radiation clock shift in Yb

K. Beloy,[1,*] J. A. Sherman,[1,2,†] N. D. Lemke,[1,2] N. Hinkley,[1,2] C. W. Oates,[1] and A. D. Ludlow[1]

[1]*National Institute of Standards and Technology, 325 Broadway, Boulder, Colorado 80305, USA*

[2]*Department of Physics, University of Colorado, Boulder, Colorado 80309, USA*

(Received 2 August 2012; published 29 November 2012)

The Stark shift of the ytterbium (Yb) optical clock transition due to room-temperature blackbody radiation is dominated by a static Stark effect, which was recently measured to high accuracy [J. A. Sherman *et al.*, Phys. Rev. Lett. **108**, 153002 (2012)]. However, room-temperature realization of the clock at 10^{-18} uncertainty requires a dynamic contribution to this static approximation. This dynamic term largely depends on a single electric dipole matrix element for which theoretically and experimentally derived values disagree significantly. We determine this important matrix element by two independent methods, which yield consistent values. Along with precise radiative lifetimes of $6s6p\ ^3P_1$ and $5d6s\ ^3D_1$, we report the clock shift due to an ideal 300 K blackbody environment to 0.05% precision.

DOI: 10.1103/PhysRevA.86.051404 PACS number(s): 32.60.+i, 06.30.Ft, 32.70.Cs

Alkaline-earth-metal-like atoms, such as Yb [1], Sr [2–4], and Hg [5], feature intrinsically narrow $^1S_0 \leftrightarrow {}^3P_0$ optical transitions capable of serving as stable and accurate frequency references [6] when laser cooled and held in an optical lattice trapping potential [7,8]. Accurate realization of optical clock transition frequencies advances timekeeping technology and enables new tests of physics [9,10].

Atomic frequency references are defined by ideal systems: atoms at rest in a null-field, zero-temperature environment [11]. Where physical realizations deviate from ideality, researchers must correct measured transition frequencies and, importantly, establish the uncertainty present in these corrections. Here we explore an optical clock correction important to many atomic species [12] arising from room-temperature blackbody radiation (BBR), specifically treating the case of Yb.

The polarizing effect of BBR largely mimics that of a static electric field due to the low frequency of BBR relative to optical transitions coupling to the clock states (see Fig. 1). Writing the BBR clock frequency shift [13]

$$\Delta\nu_{\mathrm{BBR}} = -\frac{1}{2}\frac{\Delta\alpha(0)}{h}\langle E^2\rangle_T[1+\eta_{\mathrm{clock}}(T)], \tag{1}$$

highlights its similarity to a static Stark shift, where $\Delta\alpha(0)$ is the differential *static* polarizability between clock states $|g\rangle \equiv |6s^2\ ^1S_0\rangle$ and $|e\rangle \equiv |6s6p\ ^3P_0\rangle$, $\langle E^2\rangle_T \approx (8.3193\mathrm{V/cm})^2(T/300\mathrm{K})^4$ is the time-averaged electric field intensity of BBR at absolute temperature T [14], and a small dynamic factor η_{clock} accounts for the frequency dependence of $\Delta\alpha(\omega)$. The differential static polarizability has recently been measured to high accuracy [15] (a.u. indicates atomic units [16]),

$$\Delta\alpha(0) \equiv \alpha_e(0) - \alpha_g(0) = 145.726(3)\,\mathrm{a.u.} \tag{2}$$

In practice, an imprecise thermal environment adds uncertainty to $\Delta\nu_{\mathrm{BBR}}$; an effective temperature uncertainty of 1 K due to nonuniformity sets a clock uncertainty of 3.3×10^{-17}. But this uncertainty is readily reduced by enclosing the atomic sample in a radiation shield at a well-defined temperature [3,17], a technique being developed for room-temperature or cryogenic operation.

Here we focus on a critical limitation set by the dynamic term η_{clock}. As one may infer from Fig. 1, this factor depends strongly on a single electric dipole matrix element, the $6s6p\ ^3P_0 \leftrightarrow 5d6s\ ^3D_1$ coupling [13]:

$$\mathcal{D} \equiv |\langle 6s6p\ ^3P_0||\mathbf{D}||5d6s\ ^3D_1\rangle|.$$

However, a measurement [18] and recent precise calculation [19] yield significantly different values for $\mathcal{D}$, resulting in a 1×10^{-17} clock uncertainty. Here we present two distinct determinations of $\mathcal{D}$. First, we describe a semiempirical technique that combines existing polarizability data with atomic theory to constrain $\mathcal{D}$. Then we describe a $5d6s\ ^3D_1$ radiative lifetime measurement. $5d6s\ ^3D_1$ decays predominantly to the $6s6p\ ^3P_J$ manifold, so $\mathcal{D}$ is readily extracted. Finally, we discuss how these determinations reduce the ultimate uncertainty of $\Delta\nu_{\mathrm{BBR}}$ at room temperature by an order of magnitude.

Method I: Semiempirical technique. Accurately measured experimental parameters, such as the differential static polarizability [Eq. (2)], also depend on electric dipole coupling between $6s6p\ ^3P_0$ and $5d6s\ ^3D_1$ and subsequently can be used to constrain the value of $\mathcal{D}$ [20]. The dynamic polarizability of clock state n is

$$\alpha_n(\omega) = \frac{1}{\hbar}\frac{2}{3}\sum_{n'\neq n}|\langle n'||\mathbf{D}||n\rangle|^2\frac{\omega_{n'n}}{\omega_{n'n}^2-\omega^2}, \tag{3}$$

where $\omega/2\pi$ is the frequency of the perturbing radiation, $\langle n'||\mathbf{D}||n\rangle$ is a reduced electric dipole matrix element, and $\omega_{n'n}/2\pi$ is the corresponding transition frequency. The sum over intermediate states n' implicitly includes integration over continuum states. Taking $\omega\to0$ recovers the familiar static polarizability expression.

The so-called magic trapping frequency ω^*, which balances the polarizabilities of the clock states [6],

$$\Delta\alpha(\omega^*) \equiv \alpha_e(\omega^*) - \alpha_g(\omega^*) = 0, \tag{4}$$

*kyle.beloy@nist.gov
†jeff.sherman@nist.gov

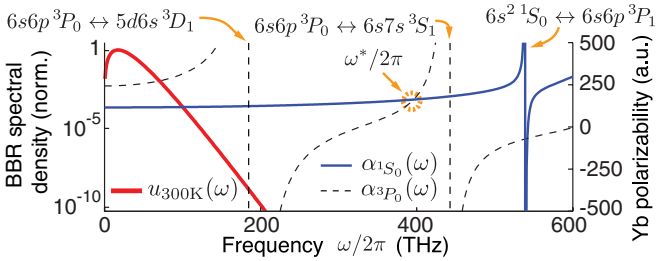

FIG. 1. (Color online) Most of the room-temperature BBR energy spectrum (thick red line) is far infrared of transitions involving the clock states. The states' polarizabilities [see Eq. (3)], largely constant over much of the BBR spectrum, are balanced at the "magic" trapping frequency ω^*.

has also been measured to high accuracy [1,21]. Equations (2) and (4) may be combined to yield

$$\Delta\alpha(0) + b\,\Delta\alpha(\omega^*) = 145.726(3)\ \text{a.u.}, \tag{5}$$

where b can be freely varied, as seen below, to enhance or suppress relative contributions of individual terms in Eq. (3). Choosing b to maximize the $6s6p\,^3P_0 \to 5d6s\,^3D_1$ contribution while simultaneously minimizing the contribution of all poorly known terms allows a precise determination of $\mathcal{D}$. Using Eq. (3), the left-hand side of Eq. (5) can be written explicitly for each clock state as

$$\alpha_n(0) + b\,\alpha_n(\omega^*) = \frac{1}{\hbar}\frac{2}{3}\sum_{n'\neq n} |\langle n'||\mathbf{D}||n\rangle|^2 \frac{1}{\omega_{n'n}} \times \left(1 + b\frac{\omega_{n'n}^2}{\omega_{n'n}^2 - \omega^{*2}}\right). \tag{6}$$

The parameter b enters only in the term in parentheses; this term acts as a "scale factor" weighting the contribution of each intermediate state in the summation. One develops an intuition with the choice $b = -1$: the scale factor tends to zero for $\omega_{n'n} \gg \omega^*$ because high-lying transitions contribute nearly identically to both $\alpha_n(0)$ and $\alpha_n(\omega^*)$. We find an advantage in choosing a value $b \approx -1$ such that both higher-lying and certain low-lying transitions are suppressed in the linear combination $\Delta\alpha(0) + b\,\Delta\alpha(\omega^*)$. Table I presents contributions to Eq. (6) for both clock states using an optimal value $b = -0.75$ as well as a pedagogically interesting value $b = 0$. In each case, we write the $6s6p\,^3P_0 \to 5d6s\,^3D_1$ contribution in terms of an unspecified matrix element $\mathcal{D}$. Contributions from other low-lying transitions are derived from experimental lifetimes [22–24]. $6s6p\,^3P_0 \to 6p^2\,^3P_1$ is an exception, as experimental data are lacking; this contribution is estimated with combined configuration interaction and many-body perturbation theory (CI + MBPT) calculations similar to Ref. [19]. This calculation does not account for potentially strong configuration mixing between $6p^2\,^3P_1$ and nearby core-excited states (see [19]), leading to a relatively large uncertainty. However, the choice $b = -0.75$ renders details of this mixing unimportant, as the suppressing scale factor in Eq. (6) becomes 0.004. Table I also displays contributions from all other transitions, including those to continuum states. While uncertainty in these contributions is also relatively large, we again benefit from substantial suppression with $b = -0.75$. The scale factor in Eq. (6) is nearly zero for the lowest of these transitions (for which $\omega_{n'n} \approx 2\,\omega^*$), rising to just 0.25 for the highest-lying, least important transitions.

TABLE I. Contributions to the static polarizability $\alpha_n(0)$ and linear combination $\alpha_n(0) - 0.75\alpha_n(\omega^*)$ [refer to Eq. (6)] for the Yb clock states (a.u.). The linear combination slightly enhances the $6s6p\,^3P_0 \to 5d6s\,^3D_1$ contribution while suppressing contributions of several other transitions.

n	n'	$\alpha_n(0)$	$\alpha_n(0) - 0.75\alpha_n(\omega^*)$
$6s^2\,^1S_0$	$6s6p\,^3P_1$	2	−1
	$6s6p\,^1P_1$	100	−4
	$(4f^{13})5d6s^2\,(\frac{7}{2},\frac{5}{2})_1$	21	1
	all others	16[a]	3[a]
$6s6p\,^3P_0$	$5d6s\,^3D_1$	$20.3\mathcal{D}^2$	$26.8\mathcal{D}^2$
	$6s7s\,^3S_1$	37	−65
	$6s6d\,^3D_1$	22	−3
	$6s8s\,^3S_1$	2	0
	$6p^2\,^3P_1$	39[b]	0[b]
	all others	27[b]	3[b]

[a]Estimated from experimental bounds on polarizability [25].
[b]Present CI + MBPT, with core polarizability from [19].

Tallying all contributions, we find

$$\Delta\alpha(0) - 0.75\Delta\alpha(\omega^*) = 26.8\mathcal{D}^2 - 64(8) + 0(6). \tag{7}$$

The first term on the right-hand side accounts for the $6s6p\,^3P_0 \to 5d6s\,^3D_1$ contribution. The second term, −64(8), accounts for other low-lying transitions in Table I; its uncertainty is dominated by that of the $6s7s\,^3S_1$ lifetime [24]. The third term, 0(6), accounts for all other transitions. Equating the right-hand side of (7) to experimental result (5) gives $\mathcal{D} = 2.80(7)$ a.u. Choices of b ranging over $(-1, -0.5)$ yield similar $\mathcal{D}$, but with uncertainties up to 40% larger. As $b \to -1$, uncertainty from the $6s7s\,^3S_1$ lifetime dominates, whereas for $b \to -0.5$, uncertainty from high-lying $6s6p\,^3P_0$ transitions dominates. We compare this result for $\mathcal{D}$ with other determinations and new data below.

Method II: Radiative lifetime. Alternatively, measurement of the $5d6s\,^3D_1$ radiative lifetime τ_a yields $\mathcal{D}$ by the traditional relation $\mathcal{D}^2 = (3\pi\epsilon_0\hbar c^3\zeta_0)(2J'+1)/(\omega_0^3\tau_a)$, where $J' = 1$; $\omega_0/2\pi \approx 2.1587 \times 10^{14}$ Hz and $\zeta_0 = 0.64(1)$ are the radiated frequency and branching ratio to $^3P_0$, respectively. Configuration mixing is small in these states [26], allowing ζ_0 to be accurately computed from LS coupling. We measure τ_a by observing population decay through the cascaded sequence $5d6s\,^3D_1 \to 6s6p\,^3P_1 \to 6s^2\,^1S_0$ [see Fig. 2(a)]. The second decay yields a 556-nm photon that is technically easier to detect than the first radiated (infrared) photon [18]. If atoms are excited at time t_0 to $^3D_1$, fluorescence from $^3P_1$ follows a double exponential [18,27],

$$y(t) = A \times \Theta(t - t_0)[e^{-(t-t_0)/\tau_a} - e^{-(t-t_0)/\tau_b}] + y_0, \tag{8}$$

where τ_b is the radiative lifetime of $^3P_1$ ($\tau_b > \tau_a$), A is a scaling factor, and y_0 accounts for stray light. The Heaviside unit step $\Theta(t - t_0)$ models instantaneous excitation at t_0. Other states populated by the decay ($^3P_0$ and $^3P_2$) are long-lived. Branching to $^3P_{0,2}$ affects only the normalization of Eq. (8), not its time dependence [28].

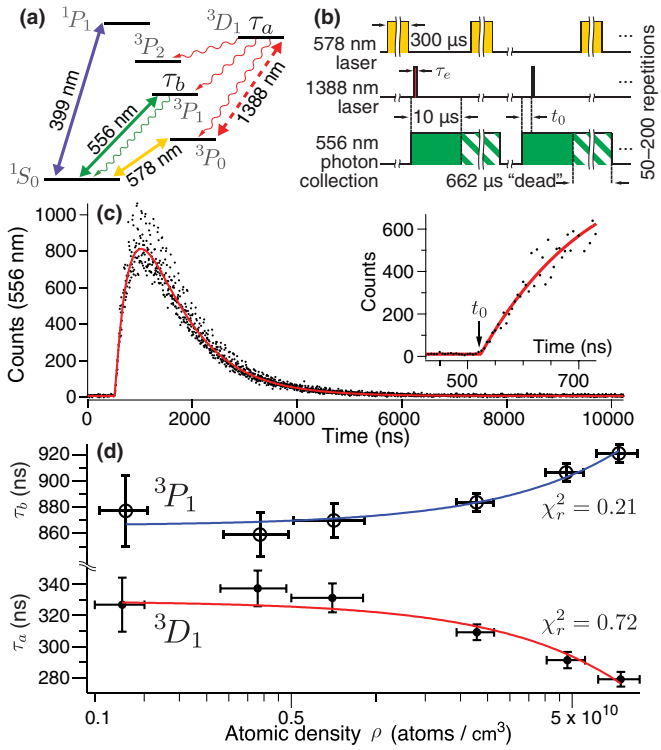

FIG. 2. (Color online) The $5d6s\ ^3D_1$ radiative lifetime via cascade decay. (a) Key lifetimes are labeled τ_a and τ_b. Double-arrowed lines indicate laser transitions. Wavy lines are important decay channels. (b) A representative pulse-timing diagram. (c) Fluorescence data taken at relatively high atomic density, fit (red line) to Eq. (8). The inset highlights the signal and fit near an excitation time $t_0 = 523.3(6)$ ns. (d) Observed lifetimes vary with atomic density ρ. Lines are linear-regression fits. Plotting the data on a logarithmic axis emphasizes data at low ρ with negligible interaction effects. Error bars represent standard uncertainties obtained from nonlinear fits and uncertainty in ρ estimates.

Laser cooling collects ^{171}Yb atoms ($N_{at} \approx 10^4$, $T_{at} \approx 10\ \mu$K) in a one-dimensional optical lattice [1]. A resonant "π pulse" of 578-nm light [29] coherently transfers atoms from $^1S_0$ to long-lived $^3P_0$ [see Fig. 2(b)]. Then, a brief ($\tau_e = 25$ ns) resonant 1388-nm pulse excites more than half of these atoms to $^3D_1$. As atoms spontaneously decay to $^1S_0$, an event counter accumulates the arrival times of radiated 556-nm photons into 5-ns bins. To increase the decay signal, this excitation and decay process can be repeated hundreds of times on the cold, lattice-trapped atoms. Though excitation occurs in the Lamb-Dicke regime, photon scattering causes heating. This heating, background gas collisions, and accumulation in $^3P_2$ limit the repetitions per loading cycle to ~200. We typically collect $1.5N_{at} \times 10^{-5}$ photons per excitation [30]. Photon "pileup" in counter bins is negligible. Between 10^6–10^7 excitations yield satisfactory decay profiles [Fig. 2(c)].

We fit fluorescence signals to Eq. (8) with a Levenberg-Marquardt routine assuming Poissonian statistical weighting. Although covariance in A, τ_a, and τ_b can be sizable, simulations establish that fitting biases become negligible with sufficiently high count totals. A maximum-likelihood method also assuming a Poissonian distribution yielded statistically similar fits.

Atomic interactions (e.g., collective emission via super- or subradiance and radiation trapping) may influence radiative decay. We probed these effects by varying the atomic density ρ undergoing decay [42]. Results [Fig. 2(d)] indicate non-negligible shortening of τ_a at the highest densities; however, the effect is negligible over the lowest decade of examined densities. In the limit of slow dipole dephasing [43], superradiance may shorten an observed lifetime as $\tau = \tau_0(1 + \rho L\lambda^2/4)^{-1}$, where τ_0 is the single-atom value, L is the length of a pencil-shaped atom cloud, and λ is the radiated wavelength [44]. For $\rho \approx 10^9\text{cm}^{-3}$ and $L \approx 0.1$ mm, the modification in this simple model is about 5%. We also saw the opposite trend in the $^3P_1$ decay, an *increase* of τ_b at high ρ. We explored both effects by varying 578- and 1388-nm pulse areas, altering the populations of $^1S_0$, $^3P_0$, and $^3D_1$, but we observed no clear trends. For the relevant densities and time scale, quenching due to cold collisions and lattice photon scattering is expected to be negligible.

Potential systematic effects arise from nonzero 1388-nm pulse duration τ_e and spurious excitation during the cascade decay caused by poor extinction of the 1388-nm laser. Therefore, we strived for fast actuation and high (60 dB) extinction of the 1388-nm light. First, a single-mode fiber-coupled mechanical shutter (500-μs rise time) precedes a fiber-coupled acousto-optic modulator (AOM). Then, a second (free space) AOM, driven with a tuned delay, aids in pulse shaping and extinction. This AOM detunes scattered light from resonance, increasing the effective extinction. With 1 mW of incident 1388-nm light focused to 30 μm ($I \approx 7 \times 10^5$ W/m^2), we attain a Rabi frequency $\Omega \propto \sqrt{I\mathcal{D}}$ exceeding 1 GHz. We detected no changes to τ_a and τ_b when varying 1388-nm intensity by 4 dB to test for dependence on Ω and stray light intensity. Likewise, we observed no systematic effect by varying τ_e from 25 to 90 ns.

We selectively excited atoms to either of the hyperfine components $^3D_1(F' = \frac{1}{2}, \frac{3}{2})$, which are split by 3.07(7) GHz. We observed no hyperfine interference beats [45] due to the large splitting and selective laser excitation. We observed no Zeeman interference oscillations [18] or significantly different results when an applied magnetic field $\vec{B}$ was varied from 0.01 to 0.1 mT. The 1388-nm light propagated along the lattice axis and was polarized perpendicular to $\vec{B}$. We detected 556-nm photons ≈45° from the lattice axis with largely

TABLE II. Uncertainty in τ_a and τ_b from atomic interactions is largely statistical as we extrapolate to zero density. We estimate fit biases and distortions due to Zeeman oscillations from Monte Carlo simulations. Uncertainties due to 1388-nm pulse duration and stray light are statistically limited.

	$u(\tau_a)$ (ns)	$u(\tau_b)$ (ns)
Atomic interactions	4.3	3.3
Fit biases	0.9	1.5
Zeeman quantum beats	3.0	3.0
1388-nm finite excitation	3.3	4.3
1388-nm stray light	3.4	4.6
Event counter timing	0.2	0.4
Total (quadrature sum)	7.1	7.4

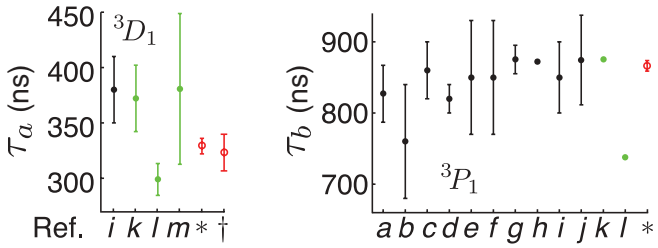

FIG. 3. (Color online) The present measurement (∗) and semiempirical result (†) are compared to other determinations. Measurements *a*–*j* are from, respectively, [31–38], [18], [39]. Points *k*–*m* are calculations from [40], [19], and [41]. When necessary, we infer lifetimes from matrix elements or natural linewidths. We assign an error bar to the τ_a from *l* using the authors' uncertainty estimate of a highly correlated polarizability.

polarization-insensitive optics. We observed a slight dependence on the number of excitations per trap cycle but attribute this effect to atomic interactions since scattering progressively reduces the atom number. Varying the lattice laser intensity over 50% yielded no significant change in observed lifetimes.

We report the radiative lifetimes $\tau_a = (329.3 \pm 7.1)$ ns and $\tau_b = (866.1 \pm 7.4)$ ns; Table II lists measurement uncertainties. Figure 3 plots our results; τ_b agrees with prior measurements, and τ_a lies between the only other measurement [18] and recent calculation [19]. Our semiempirical determination (method I) agrees well with our experimental measurement (method II). Table III lists the results as inferred matrix elements.

BBR clock shift. The BBR Stark shift to the clock frequency is found from the expression

$$\Delta\nu_{\mathrm{BBR}} = -\frac{1}{2h\epsilon_0}\int_0^\infty u_T(\omega)\,\Delta\alpha(\omega)\,d\omega, \tag{9}$$

where $u_T(\omega)$ is the BBR spectral energy density corresponding to temperature T, given by Planck's law. A static approximation neglecting the slight frequency dependence of $\Delta\alpha(\omega)$ over the BBR spectrum (see Fig. 1) is formally obtained by substituting $\Delta\alpha(\omega) \to \Delta\alpha(0)$ in Eq. (9). An improved approximation adds the lowest-order frequency dependence of the differential polarizability due to the $6s6p\,^3P_0 \to 5d6s\,^3D_1$ transition: $\Delta\alpha(\omega) \to \Delta\alpha(0) + (2/3\hbar)(\mathcal{D}^2/\omega_0^3)\omega^2$. Integrating over ω analytically, we interpret the additional shift as $\eta_{\mathrm{clock}}(T) \approx \frac{80\pi^2}{63}\frac{\mathcal{D}^2}{(\hbar\omega_0)^3}\frac{(k_BT)^2}{\Delta\alpha(0)} \approx 0.017(\frac{T}{300\mathrm{K}})^2$ from Eq. (1), where k_B is Boltzmann's constant. A thorough account of small contributions from all other transitions, including $^1S_0$ and next-order terms ($\propto T^4$) yields [46]

$$\eta_{\mathrm{clock}}(T) = 0.0173(5)\left(\frac{T}{300\,\mathrm{K}}\right)^2 + 0.0006\left(\frac{T}{300\,\mathrm{K}}\right)^4.$$

Uncertainty in the second term here is negligible. Higher-order terms ($\propto T^6, T^8, \ldots$) may be omitted at our level of accuracy. We estimate that magnetic dipole coupling to the BBR field gives a negligible ($\sim 1 \times 10^{-5}$) contribution to η_{clock} at room temperature, with higher multipolar contributions being suppressed further [13].

TABLE III. The present results, expressed as reduced matrix elements (a.u.), are compared with selected literature values.

	$\mathcal{D}$	$\lvert\langle 6s6p\,^3P_1\rvert\rvert\mathbf{D}\rvert\rvert 6s^2\,^1S_0\rangle\rvert$
Experiment	2.77(4)	0.542(2)
Semiempirical	2.80(7)	
Experiment [18]	2.58(10)	0.547(16)
Calculation [40]	2.61(10)	0.54(8)
Calculation [19]	2.91(7)	0.587
Calculation [41]	2.58(23)	0.41(1)

A semiempirical analysis and radiative lifetime measurement, techniques generally applicable to all atomic species including alkaline-earth-metal-like clock atoms, has yielded atomic structure information relevant to the BBR shift in the Yb optical frequency reference. In an ideal 300 K BBR environment, we use the present results to calculate $\Delta\nu_{\mathrm{BBR}} = -1.2774(6)$ Hz. This determination of η_{clock} allows for high-accuracy clock operation at room temperature, contributing 1.1×10^{-18} to the clock uncertainty. To match this accuracy, the effective temperature of the environment needs to be known to 35 mK. Alternatively, cryogenic clock operation would reduce the uncertainty contribution of η_{clock} to negligible levels while also reducing the need for high-accuracy temperature control.

Note added. We recently became aware of works presenting η_{clock} for Yb [47] and Sr [48]. The *ab initio* theoretical treatment [47] agrees with the present results.

Acknowledgements. We acknowledge NIST, DARPA QuASAR, NASA, and NRC-RAP for financial support. We thank J. Ye and J. Bergquist for loaning equipment, A. Derevianko and V. Dzuba for useful discussions, N. Phillips for laboratory contributions, and P. Del'Haye and R. Mhaskar for careful reading of the manuscript.

[1] N. D. Lemke, A. D. Ludlow, Z. W. Barber, T. M. Fortier, S. A. Diddams, Y. Jiang, S. R. Jefferts, T. P. Heavner, T. E. Parker, and C. W. Oates, Phys. Rev. Lett. **103**, 063001 (2009).

[2] R. Le Targat, X. Baillard, M. Fouché, A. Brusch, O. Tcherbakoff, G. D. Rovera, and P. Lemonde, Phys. Rev. Lett. **97**, 130801 (2006).

[3] A. D. Ludlow, T. Zelevinsky, G. K. Campbell *et al.*, Science **319**, 1805 (2008).

[4] S. Falke, H. Schnatz, J. Winfred *et al.*, Metrologia **48**, 399 (2011).

[5] J. J. McFerran, L. Yi, S. Mejri, S. Di Manno, W. Zhang, J. Guéna, Y. Le Coq, and S. Bize, Phys. Rev. Lett. **108**, 183004 (2012).

[6] A. Derevianko and H. Katori, Rev. Mod. Phys. **83**, 331 (2011).

[7] S. G. Porsev, A. Derevianko, and E. N. Fortson, Phys. Rev. A **69**, 021403 (2004).

[8] M. Takamoto, F. L. Hong, R. Higashi, and H. Katori, Nature (London) **435**, 321 (2005).
[9] S. Blatt, A. D. Ludlow, G. K. Campbell *et al.*, Phys. Rev. Lett. **100**, 140801 (2008).
[10] T. Rosenband, D. B. Hume, P. O. Schmidt *et al.*, Science **319**, 1808 (2008).
[11] *The International System of Units (SI)*, edited by B. N. Taylor and A. Thompson, NIST Special Publication 330 (U.S. Department of Commerce, National Institute of Standards and Technology, Gaithersburg, MD, 2008).
[12] J. Mitroy, M. Safronova, and C. Clark, J. Phys. B **43**, 202001 (2010).
[13] S. G. Porsev and A. Derevianko, Phys. Rev. A **74**, 020502 (2006).
[14] E. J. Angstmann, V. A. Dzuba, and V. V. Flambaum, Phys. Rev. A **74**, 023405 (2006).
[15] J. A. Sherman, N. D. Lemke, N. Hinkley, M. Pizzocaro, R. W. Fox, A. D. Ludlow, and C. W. Oates, Phys. Rev. Lett. **108**, 153002 (2012).
[16] The atomic unit for polarizability is 1 a.u. $= 0.2488319 \times h \times$ mHz $(\mathrm{V/cm})^{-2}$, where h is Planck's constant. Expressed in atomic units, $e = m_e = \hbar = 4\pi\epsilon_0 = 1$ [12].
[17] T. Middelmann, C. Lisdat, S. Falke, J. Vellore Winfred, F. Riehle, and U. Sterr, IEEE Trans. Instrum. Meas. **99**, 1 (2011).
[18] C. J. Bowers, D. Budker, E. D. Commins, D. DeMille, S. J. Freedman, A.-T. Nguyen, S.-Q. Shang, and M. Zolotorev, Phys. Rev. A **53**, 3103 (1996).
[19] V. A. Dzuba and A. Derevianko, J. Phys. B **43**, 074011 (2010).
[20] S. G. Porsev, A. D. Ludlow, M. M. Boyd, and J. Ye, Phys. Rev. A **78**, 032508 (2008).
[21] Z. W. Barber, J. E. Stalnaker, N. D. Lemke, N. Poli, C. W. Oates, T. M. Fortier, S. A. Diddams, L. Hollberg, C. W. Hoyt, A. V. Taichenachev, and V. I. Yudin, Phys. Rev. Lett. **100**, 103002 (2008).
[22] Y. Takasu, K. Komori, K. Honda, M. Kumakura, T. Yabuzaki, and Y. Takahashi, Phys. Rev. Lett. **93**, 123202 (2004).
[23] K. B. Blagoev and V. A. Komarovskii, At. Data Nucl. Data Tables **56**, 1 (1994).
[24] M. Baumann, M. Braun, A. Gaiser, and H. Liening, J. Phys. B **18**, L601 (1985).
[25] K. Beloy, Phys. Rev. A **86**, 022521 (2012).
[26] W. Martin, R. Zalubas, and L. Hagan, *Atomic Energy Levels—The Rare-Earth Elements* (National Bureau of Standards, US Department of Commerce, Washington, DC, 1978).
[27] D. Budker, D. DeMille, E. D. Commins, and M. S. Zolotorev, Phys. Rev. A **50**, 132 (1994).
[28] D. Budker, D. Kimball, and D. DeMille, *Atomic Phyiscs: An Exploration through Problems and Solutions* (Oxford University Press, Oxford, 2004).
[29] Y. Y. Jiang, A. D. Ludlow, N. D. Lemke, R. W. Fox, J. A. Sherman, L.-S. Ma, and C. W. Oates, Nat. Photonics **5**, 158 (2011).
[30] A lens capturing 0.14 sr collects atomic fluorescence through a beam splitter onto photomultiplier tubes configured for 556- and 399-nm detection. A multichannel scaler/averager (Stanford Research Systems SR430) discriminates and accumulates time-resolved photon counts.
[31] M. Baumann and G. Wandel, Phys. Lett. **22**, 283 (1966).
[32] B. Budick and J. Snir, Phys. Rev. A **1**, 545 (1970).
[33] W. Gornik, D. Kaiser, W. Lange, J. Luther, and H. Schulz, Opt. Commun. **6**, 327 (1972).
[34] F. H. K. Rambow and L. D. Schearer, Phys. Rev. A **14**, 738 (1976).
[35] M. L. Burshtein, Y. F. Verolainen, V. A. Komarovskii, A. L. Osherovich, and N. P. Penkin, Opt. Spectrosc. **37**, 351 (1974).
[36] K. B. Blagoev, V. A. Komarovskii, and N. P. Penkin, Opt. Spectrosc. **45**, 832 (1978).
[37] M. Gustavsson, H. Lundberg, L. Nilsson, and S. Svanberg, J. Opt. Soc. Am. **69**, 984 (1979).
[38] J. E. Golub, Y. S. Bai, and T. W. Mossberg, Phys. Rev. A **37**, 119 (1988).
[39] M. Kitagawa, K. Enomoto, K. Kasa, Y. Takahashi, R. Ciuryło, P. Naidon, and P. S. Julienne, Phys. Rev. A **77**, 012719 (2008).
[40] S. G. Porsev, Y. G. Rakhlina, and M. G. Kozlov, Phys. Rev. A **60**, 2781 (1999).
[41] K. Guo, G. Wang, and A. Ye, J. Phys. B **43**, 135004 (2010).
[42] Here, ρ is the mean density averaged over the lattice sites and throughout the repeated cascade decay sequence [see Fig. 2(b)]. ρ is measurable by inserting resonant 399-nm pulses into the sequence. After subtracting the background, we assume 399-nm fluorescence is $\propto \rho$. In the low-ρ regime, density inhomogeneity is unimportant.
[43] The dephasing time scale in cold trapped atoms is likely set by inhomogeneous ac Stark shifts. We estimate $T_2^* \approx 5\ \mu$s, which is somewhat longer than τ_a and τ_b.
[44] M. Gross, C. Fabre, P. Pillet, and S. Haroche, Phys. Rev. Lett. **36**, 1035 (1976).
[45] S. Haroche, J. Paisner, and A. Schawlow, Phys. Rev. Lett. **30**, 948 (1973).
[46] See Supplemental Material at http://link.aps.org/supplemental/10.1103/PhysRevA.86.051404 for tabulated contributions to atomic response factors (e.g., polarizabilities and the BBR dynamic correction factor).
[47] M. S. Safronova, S. G. Porsev, and C. W. Clark, arXiv:1208.1456.
[48] T. Middelmann, S. Falke, C. Lisdat, and U. Sterr, arXiv:1208.2848.